Mon. Not. R. astr. Soc. (1984) **206**, 407–422

Magnetic field distributions in white dwarfs

Brian Martin and D. T. Wickramasinghe
Department of Mathematics, Faculty of Science, Australian National University, GPO Box 4, Canberra ACT 2601, Australia

Received 1983 June 6; in original form 1983 January 26

Summary. The sensitivity of the spectroscopic and polarimetric properties of magnetic white dwarfs to field geometry is investigated using uniform, dipole, quadrupole, octupole and two offset dipole models. The results suggest that often it may be difficult to distinguish between an offset dipole and a combination of multipoles, as in the case of GD90. The effect of line broadening on the spectra of magnetic white dwarfs is also investigated.

1 Introduction

Angel (1978) and Landstreet (1979) have discussed a number of white dwarf stars with high magnetic fields ($B > 10^6$ G). The high field is inferred either from significant values of circular polarization or from the shifting and splitting of absorption lines (Zeeman splitting). In a series of papers we have developed realistic models for such stars, with realistic stellar atmospheres and the use of realistic line profiles in a full integration of the radiative transfer equations in a magnetic field through the appropriate optical depths and across the surface of the star. Our early models reproduced many of the features of the stars BPM 25114, GD90 and G99 – 47 (Martin & Wickramasinghe 1978; Wickramasinghe & Martin 1979) and presented many of the general features of such models (see also O'Donoghue 1980).

There are quite a few assumptions and further effects which need to be examined before all magnetic white dwarf spectra can be explained, and general conclusions can be reached regarding the magnetic field structure. One important effect at very high magnetic fields ($B \gtrsim 10^8$ G) is cyclotron absorption (Martin & Wickramasinghe 1979a). Also important in explaining the details of magnetic white dwarf spectra, especially linear and circular polarization, are magneto-optical effects associated with bound–free and free–free transitions (Martin & Wickramasinghe 1981, 1982). In spite of being relatively realistic, our models still include a number of simplifications and approximations. In particular, we treat the hydrogen line profiles as Voigt profiles with the damping parameter as an undetermined parameter, assume that the temperature structure of the model is unaffected by the magnetic field, that

the abundances assumed in the model atmospheres are appropriate and that the Balmer lines are not appreciably affected by non-LTE effects.

In this paper we examine in some detail the effect of the magnetic field geometry on the spectra of magnetic white dwarfs, and also investigate the relative importance of pressure and magnetic hardening. Almost all previous studies have assumed initially a dipole field coincident with the centre of the star. Sometimes the dipole is offset from the centre of the star, if this seems useful in improving agreement between model and observations, as we found in the case of GD90 (Wickramasinghe & Martin 1979). Earlier studies (Kemic 1974a; Borra 1976; Wegner 1977) have produced line and circular polarization profiles for absorption lines, but these calculations use simplifications such as the simple Unno (1956) solution to the radiative transfer equations and a Milne–Eddington model atmosphere, rather than the realistic atmosphere and full numerical solution to the radiative transfer equations used here.

There are some theoretical reasons to expect dipole fields to be most common among magnetic white dwarfs, since in their long lifetime the higher moments of the magnetic field tend to die away. However, in the hotter and younger stars, a significant non-dipole component could be present, particularly if the fields originate by the dynamo mechanism in convective stellar cores during later stages of evolution as proposed by Ruderman & Sutherland (1973) (see Liebert *et al.* 1977 for a discussion). The inference of field structure from observations and models is thus important for the theory of the origin of magnetic fields in white dwarfs.

Here we aim to give a feeling for the spectra arising from a variety of field geometries. For this purpose we have selected a uniform, centred dipole, quadrupole and octupole fields, and two different offset dipole fields. In each of these cases we present information about the distribution of field strengths, and illustrate the effect of these field geometries on a standard Hα line. We also show the effect of line broadening on the spectra. Finally, models for GD90 are examined to determine whether the limited data available provides sufficient information to distinguish dipole from non-dipole field geometries.

Some of the work here parallels studies of magnetic Ap and Bp stars which also address the issue of field distributions (see the review by Landstreet 1980).

2 Radiative transfer

The equations for radiative transfer in a magnetic field may be written (Hardorp, Shore & Wittmann 1976):

$$\mu \frac{dI}{d\tau} = \eta_I (I-B) + \eta_Q Q + \eta_V V, \tag{1}$$

$$\mu \frac{dQ}{d\tau} = \eta_Q (I-B) + \eta_I Q - \rho_R U, \tag{2}$$

$$\mu \frac{dU}{d\tau} = \rho_R Q + \eta_I U - \rho_W V, \tag{3}$$

$$\mu \frac{dV}{d\tau} = \eta_V (I-B) + \rho_W U + \eta_I V. \tag{4}$$

Here I, Q, U and V are the four Stokes parameters, τ is the optical depth, B is the local source function (elsewhere in this paper B represents magnetic field), $\mu = \cos\theta$ where θ is

the angle between the propagation direction and the normal to the surface of the star, and

$$\eta_I = \tfrac{1}{2}\eta_p \sin^2\psi + \tfrac{1}{4}(\eta_l + \eta_r)(1 + \cos^2\psi), \quad (5)$$

$$\eta_Q = [\tfrac{1}{2}\eta_p - \tfrac{1}{4}(\eta_l + \eta_r)] \sin^2\psi, \quad (6)$$

$$\eta_V = \tfrac{1}{2}(\eta_r - \eta_l)\cos\psi, \quad (7)$$

where ψ is the angle between the propagation direction and the direction of the magnetic field, η_p, η_l and η_r are the ratios of the total absorption coefficient of the three Zeeman shifted components plus the shifted continuum absorption coefficient to the unshifted absorption coefficient, and ρ_R and ρ_W introduce magneto-optical effects. The solution pair

$$\begin{pmatrix} Q \\ U \end{pmatrix}$$

to (1)–(4) must be multiplied by

$$\begin{pmatrix} \cos 2\phi & -\sin 2\phi \\ \sin 2\phi & \cos 2\phi \end{pmatrix}$$

where ϕ is the azimuth with respect to an arbitrary x-axis at right angles to the line-of-sight.

When the magnetic field is zero, $\eta_r = \eta_l = \eta_p$, hence $\eta_Q = \eta_V = 0$ and the radiative transfer equations reduce to one equation. This gives rise to the familiar absorption lines found in non-magnetic stars. When the magnetic field is non-zero, the lines can be broadened or split in two ways, which may be called line shift broadening and field spread broadening.

First consider line shift broadening. A non-zero magnetic field causes the different com-

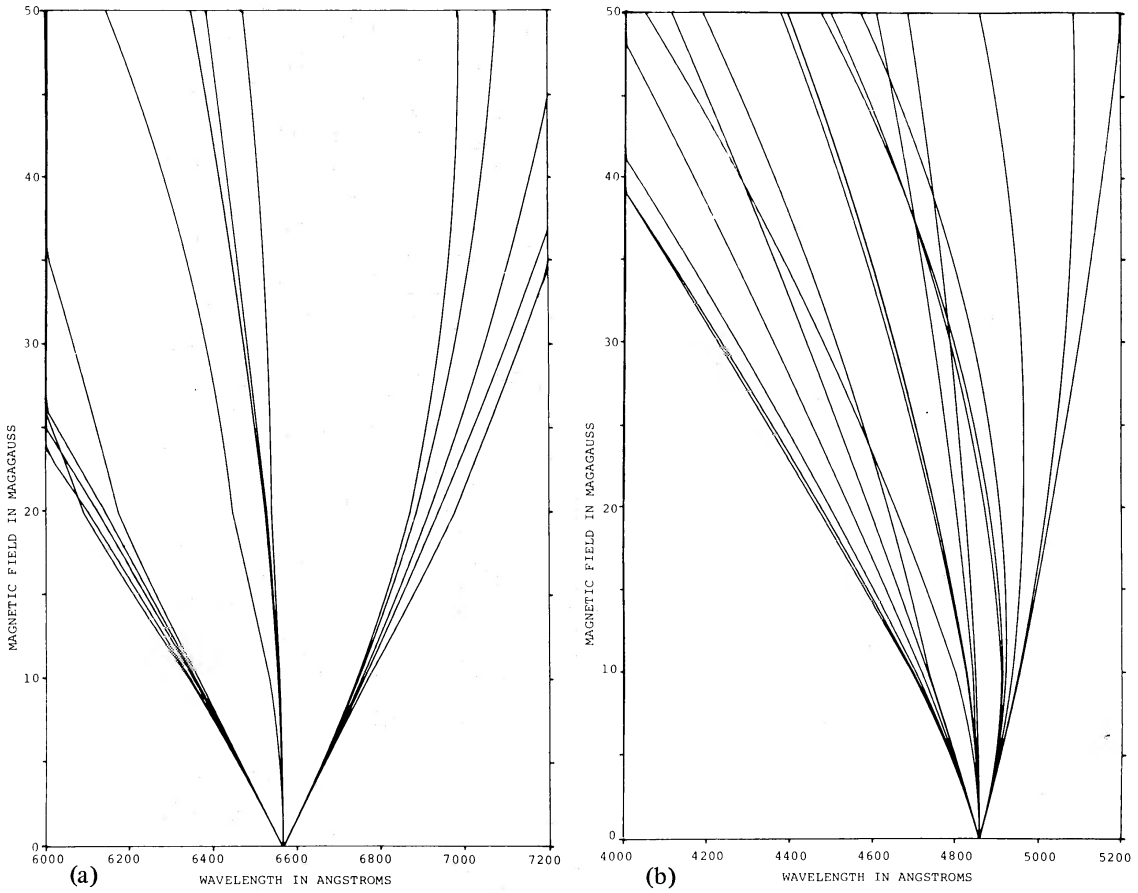

Figure 1. Magnetic splitting of (a) Hα and (b) Hβ in fields up to 50 MG. The wavelengths are interpolated from the tables of Kemic (1974b) using a quadratic fit in the magnetic field strength B.

ponents of an absorption line to shift to different wavelengths, depending on the component and the strength of the magnetic field. As seen in Fig. 1, typically the *r*, *l* and *p*-type components each shift in different characteristic ways, giving rise to the familiar Zeeman splitting. At low fields a Zeeman triplet results. Note that line shift broadening occurs even in a uniform field. In studies involving low fields, such that the line shift broadening results in a slightly broader feature but no splitting, this effect is called magnetic intensification.

The second type of line broadening in a magnetic field, which we call field spread broadening, is due to non-uniformity of the magnetic field. When the field varies across the surface of the star, any given component will be shifted by different amounts by the different fields, as seen in Fig. 1 (except in special cases in which the wavelength of absorption is not affected by the field strength). The net effect is a broadening of the feature from the component. When the field is large (e.g. 10^7G) and varies significantly across the surface of the star (as in a dipole), field spread broadening is dominant over line shift broadening. In any case, the combination of the two effects is called simply magnetic broadening.

At sufficiently large fields the magnetic broadening can dominate over the pressure broadening, so that detailed knowledge of the line profile is not required. The importance of pressure broadening at high fields is examined later in this paper.

To illustrate the effect of the magnetic field on the spectrum, consider a white dwarf with a dipole magnetic field with pole strength $B_p = 10^7$G. The field strength varies from this value at the poles down to 5×10^6G at the equator. Since areas of the star covering this full range of field strengths contribute to the spectrum, shifts in Fig. 1 from 5×10^6G to 10^7G will all play a part. For example, the centres of the *l* components of Hβ will absorb at most wavelengths between 4700 and 4800 Å.

The calculation of the emergent spectrum can be conceptualized in the way in which the computer calculation proceeds. At a given wavelength, latitude and optical depth, the magnetic field strength – which for the field distributions used here depends on latitude but not longitude – is examined to determine the appropriate component shifts. Each component is examined, and its contributions to the opacities are determined according to its deviation in angstroms from the current wavelength. Each component sufficiently near to the current wavelength thus makes a contribution to η_r, η_l or η_p, and also to ρ_R and ρ_W. The contribution depends on the optical depth through the effect of electron density and temperature on excitation and on the Stark broadening of the line. Adding continuum contributions, the final values of the opacities and magneto-optical parameters are determined. Utilizing the angle ψ between magnetic field direction and propagation direction, the values of η_I, η_Q, η_V, ρ_R and ρ_W are found and used in (1)–(4) to calculate the values of the Stokes parameters at the next optical depth towards the surface. The optical depth integration proceeds with redetermination of opacities and magneto-optical parameters at each depth. (We use the numerical method presented in Martin & Wickramasinghe 1979b.)

The calculation for different longitudes can proceed with the same opacity values, since with dipole and multipole fields only ψ and μ in the calculation are affected by the longitude. For different latitudes, different magnetic field strengths apply, and new sets of opacity and magneto-optical contributions from the line components must be determined. The calculated surface values of *I*, *Q*, *U* and *V* at the different latitude and longitude points are weighted by appropriate area and angle factors to give the net result. This process is then repeated at other wavelengths. (In practice, to save computer time, a whole series of calculations at different wavelengths is carried out in parallel, so that profiles of the components of the lines can be allocated to the full range of wavelengths in a single operation.)

The magnetic field geometry enters into this calculational procedure in two ways. First, for a given wavelength and latitude, the geometry determines the position of the centre of

each component of the line. Secondly, for a given latitude and longitude, the geometry determines the angle ψ between the field direction and the propagation direction.

3 Field geometry

A standard way of characterizing both electric and magnetic field distributions is in terms of multipoles (see, for example Cowan 1968, chapter 8). An electric or magnetic potential Φ can be expanded in terms of Legendre polynomials:

$$\Phi = \sum_{n=0}^{\infty} \frac{a_n P_n(\cos \xi)}{r^{n+1}}, \tag{8}$$

where P_n is the nth Legendre polynomial, r is the distance from the centre of the star, ξ is the angle between the north pole and the current latitude, and a_n is the coefficient of the $2n$-pole. The field of the $2n$-pole (dipole is $n = 1$, quadrupole is $n = 2$, octupole is $n = 3$, etc) is $-\nabla\Phi$, appropriately normalized. For example, for a dipole

$$\Phi_1 = \frac{\cos \xi}{r^2} = \frac{z}{r^3}$$

and

$$B_z = -\frac{\partial \Phi_1}{\partial z},$$

where we have introduced an x, y, z coordinate system with $x^2 + y^2 + z^2 = r^2$ with z the magnetic axis.

Setting $r = 1$ after results are obtained (so that $z = \cos \xi$, $x = \sin \xi \cos \zeta$ and $y = \sin \xi \sin \zeta$, where ζ is the longitude), we have

Dipole

$$B_z = B_p(3z^2 - 1)/2, \tag{9}$$

$$B_x = B_p 3xz/2, \tag{10}$$

$$B = B_p(3z^2 + 1)^{1/2}/2, \tag{11}$$

Quadrupole

$$B_z = B_p z(5z^2 - 3)/2, \tag{12}$$

$$B_x = B_p x(5z^2 - 1)/2, \tag{13}$$

$$B = B_p(5z^4 - 2z^2 + 1)^{1/2}/2, \tag{14}$$

Octupole

$$B_z = B_p(35z^4 - 30z^2 + 3)/8, \tag{15}$$

$$B_x = B_p xz(35z^2 - 15)/8, \tag{16}$$

$$B = B_p(175z^6 - 165z^4 + 45z^2 + 9)^{1/2}/8, \tag{17}$$

Uniform

$$B_z = B_p, \tag{18}$$

$$B_x = 0, \tag{19}$$

$$B = B_p. \tag{20}$$

B_p is the polar field strength, and each field is normalized such that $B_z = B_p$ when $z = 1$ [i.e. $a_n = 1/(n+1)$]. B_y is given by B_x with x replaced by y throughout. B is the total field strength: $B = (B_x^2 + B_y^2 + B_z^2)^{1/2}$. A uniform field in the z direction is given for completeness.

Another way of characterizing non-dipole magnetic field distributions, more commonly used in astrophysics than multipoles, is the offset dipole: the magnetic dipole is assumed not to emanate from the centre of the star, but from a position displaced from the centre. There are two independent directions in which this displacement or offsetting may occur, which may be taken to be along the direction of the magnetic dipole (z direction) and perpendicular to this direction (in the x–y plane). These two directions, plus the arbitrary displacements which may be made along them, allow a wide range of flexibility in producing different field distributions. Here we consider only displacements along the z axis, by distances of plus or minus 0.1 or 0.2 of the star's radius. Denoting this fractional shift by s, the distance to the surface of the star in units of the radius is

$$r_s = (1 + s^2 - 2s\cos\xi)^{1/2}. \tag{21}$$

The field direction becomes

$$\xi_s = \arcsin\,[(\sin\xi)/r_s]. \tag{22}$$

To determine values of B_z, B_x and B for the offset dipole, the equations (9)–(20) are used

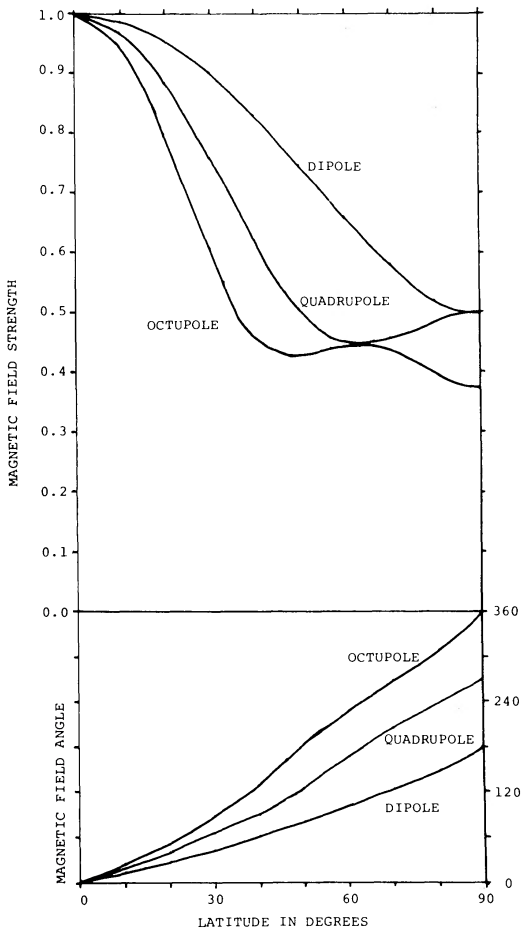

Figure 2. Variation of magnetic field strength with the angle between the pole and the current latitude (top section) and the variation of the magnetic field angle, arctan $[(B_x^2 + B_y^2)^{1/2}/B_z]$ (bottom section) for centred dipole, quadrupole and octupole fields.

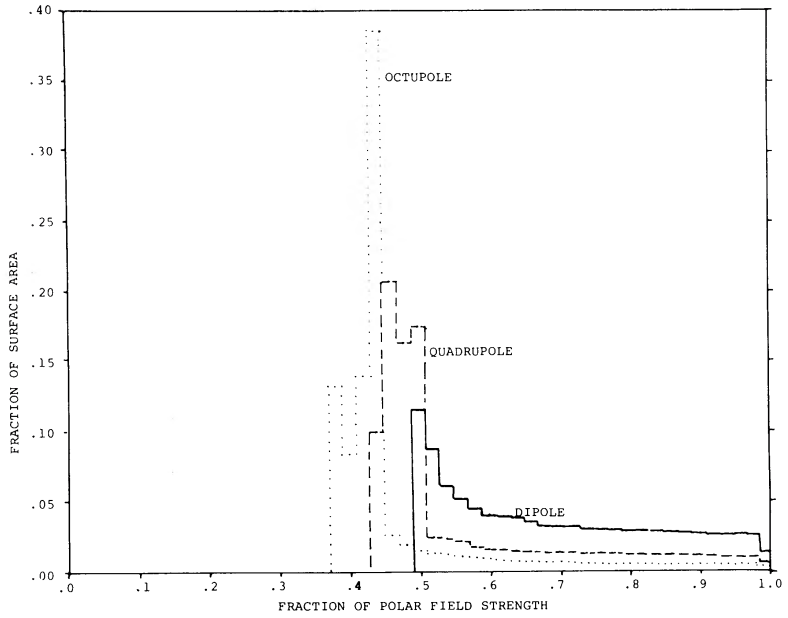

Figure 3. Histograms showing the fraction of the area of the surface of a star on which different field strengths are found, assuming either a centred dipole (solid line), quadrupole (dashed line) or octupole field (dotted line). Intervals are 0.37 to 0.39, 0.39 to 0.41, etc, of the polar field strength.

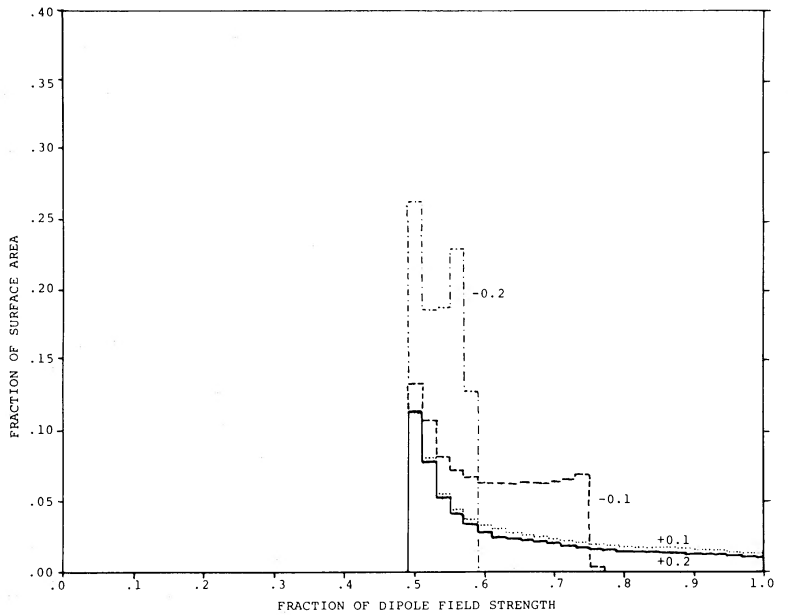

Figure 4. Histograms showing the fraction of the area of the northern hemisphere of a star on which different field strengths are found, assuming dipole fields offset by either 0.2 of the star's radius towards the north pole (solid line), 0.1 of the star's radius towards the north pole (dotted line), 0.1 of the star's radius towards the south pole (dashed line), or 0.2 of the star's radius towards the south pole (dotted and dashed line). Intervals are 0.49 to 0.51, 0.51 to 0.53, etc, of the dipole field strength. For the northerly (positively) offset dipoles, field strengths greater than the dipole field strength also occur, but are not shown.

with $z = \cos \xi$ replaced by $z_s = \cos \xi_s$, x replaced by $x \sin \xi_s / \sin \xi$, and the strength of the dipole divided by r_s^3, the quadrupole by r_s^4 and the octupole by r_s^5.

An offset dipole can be expressed as a weighted sum of multipole moments. But rather than pursue a formal analysis along these lines, we prefer to provide a basis for a more physical and intuitive understanding of the effects of different field distributions. In Fig. 2,

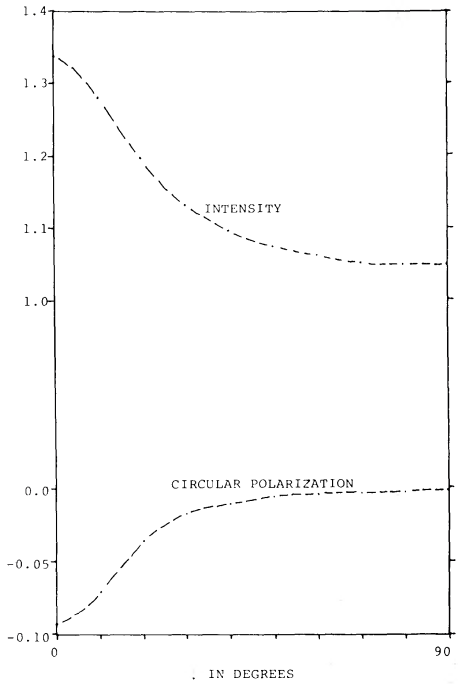

Figure 5. Solutions for intensity (I) and circular polarization (V/I) calculated from (1)–(4) at a position between two components of a Zeeman triplet, for different angles ψ between the magnetic field direction and the viewing angle. The hypothetical Zeeman triplet is calculated with $\lambda(v = 0) = 5000$ Å T–τ relation taken from the zero-field, high-gravity (log $g = 8.0$) model atmosphere for a DA white dwarf with $T_e = 20\,000$ K given by Wickramasinghe (1972), continuum opacities $\eta_p = 1.00$, $\eta_r = 1.08$, $\eta_l = 0.93$ and continuum magneto-optical parameters $\rho_R = -20\,000$, $\rho_W = -400$, all independent of optical depth, a Voigt line profile with strength $\eta_0 = 10\,000$ (see Martin & Wickramasinghe 1982 for definition) and damping parameter $a = 0.1$, Zeeman components at $v_r = -16$, $v_p = 0$ and $v_l = 16$ where v is the position within the line profile, $\mu = 0.8$ and $\cos 2\phi = 0$. Results are given for $v = -4$. Linear polarization behaves similarly to circular polarization, but has a much smaller magnitude.

the total field strength B and the field angle $\arctan[(B_x^2 + B_y^2)^{1/2}/B_z]$ are presented as functions of latitude angle for the uniform and centred dipole, quadrupole and octupole fields. In Figs 3 and 4 are histograms of field strengths found on the surface of stars with different field distributions, with each strength weighted by the fraction of the area of the surface of the star on which it appears. (These weights naturally will change when the viewing angle is taken into account.)

From (11), (14) and (17) it is easily found that the dipole ranges from the full (polar) field strength down to one half at the equator ($z = 0$), the quadrupole down to $1/5^{1/2}$ at $z = 1/5^{1/2}$, and the octupole down to 3/8 at the equator. Between the pole and the equator the dipole has one field strength maximum and one minimum, the quadrupole two local maxima and one minimum, and the octupole two maxima and two minima (see Fig. 2). The net effect is that although the higher multipoles have a greater total range of field strengths, they are more uniform overall. From Fig. 4 it is apparent that offset dipoles have a much larger range of field strengths when offset towards the hemisphere being considered, and a quite uniform range when offset in the opposite direction.

The field strengths are the main determinant of the positions of the spectral lines (Fig. 1). Figs 3 and 4 suggest that to obtain a field giving high magnetic broadening, the positively offset dipole is suitable, and to obtain a field giving magnetic splitting but less magnetic broadening, higher multipole fields or negatively offset dipoles can be used.

Although the direction of the magnetic field does not affect the position of the spectral

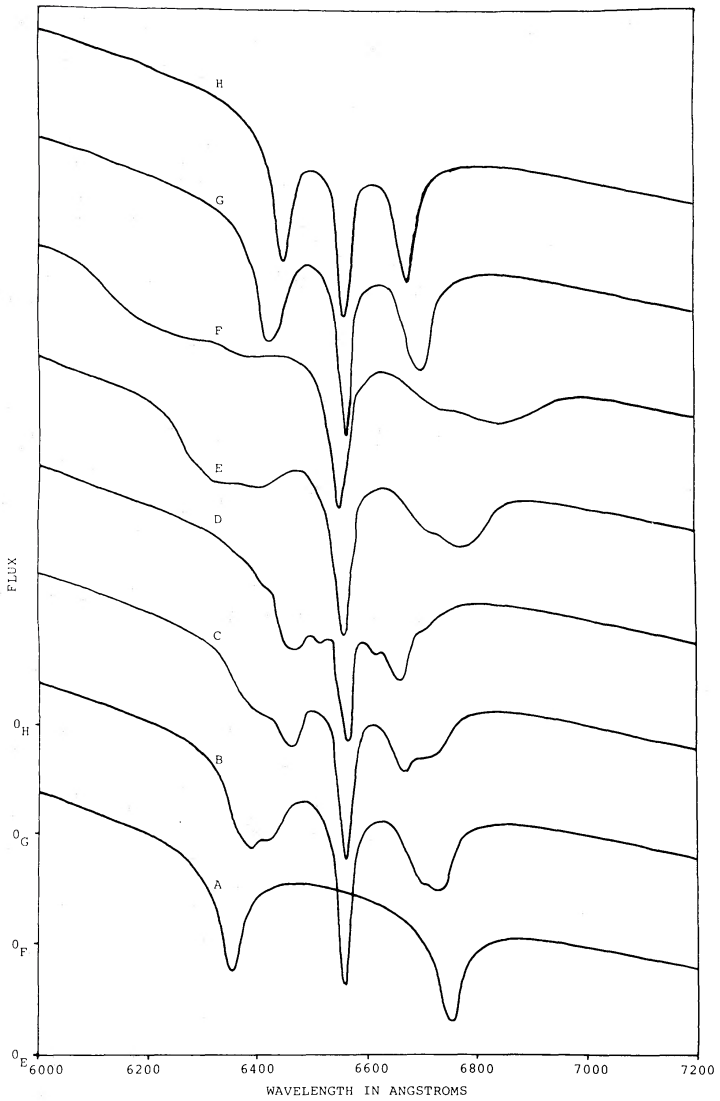

Figure 6. Values of flux for a realistic model magnetic white dwarf near the Hα absorption line for different field geometries: (A) uniform, (B) centred dipole, (C) centred quadrupole, (D) centred octupole, (E) dipole offset 0.1 towards the north pole, (F) dipole offset 0.2 towards the north pole, (G) dipole offset 0.1 towards the south pole and (H) dipole offset 0.2 towards the south pole, where the offset fractions are of the star's radius. The star is viewed from the direction of the north pole ($i = 0°$). The white dwarf model atmosphere is the zero-field, high-gravity ($\log g = 8.0$), $T_e = 20\,000$ K model taken from Wickramasinghe (1972). The damping parameter $a = 0.1$. The dipole field strength is $B_d = 10^7$G, and the polar field strength for the uniform, quadrupole and octupole fields is also $B_p = 10^7$G. The curves are spaced equally apart, and the zeros for E–H are indicated.

lines, it can affect the strength of absorption markedly. We do not present histograms of the direction of the magnetic field, since in determining the angle ψ between the propagation direction and the magnetic field direction the viewing angle i is also critical. But to indicate the importance of ψ, we present in Fig. 5 values of intensity and circular polarization for different values of ψ at a particular position in a line profile. It is apparent that the line depth is greatest near $\psi = 90°$ and least near $\psi = 0°$. Nearer the centre of the line (not shown) only a few angles near $\psi = 0°$ do not give saturation, while far from the line centre (also not shown) only a few angles near $\psi = 90°$ give much absorption at all. The different patterns of ψ generated by different field distributions thus can lead to significant differences in flux and polarization.

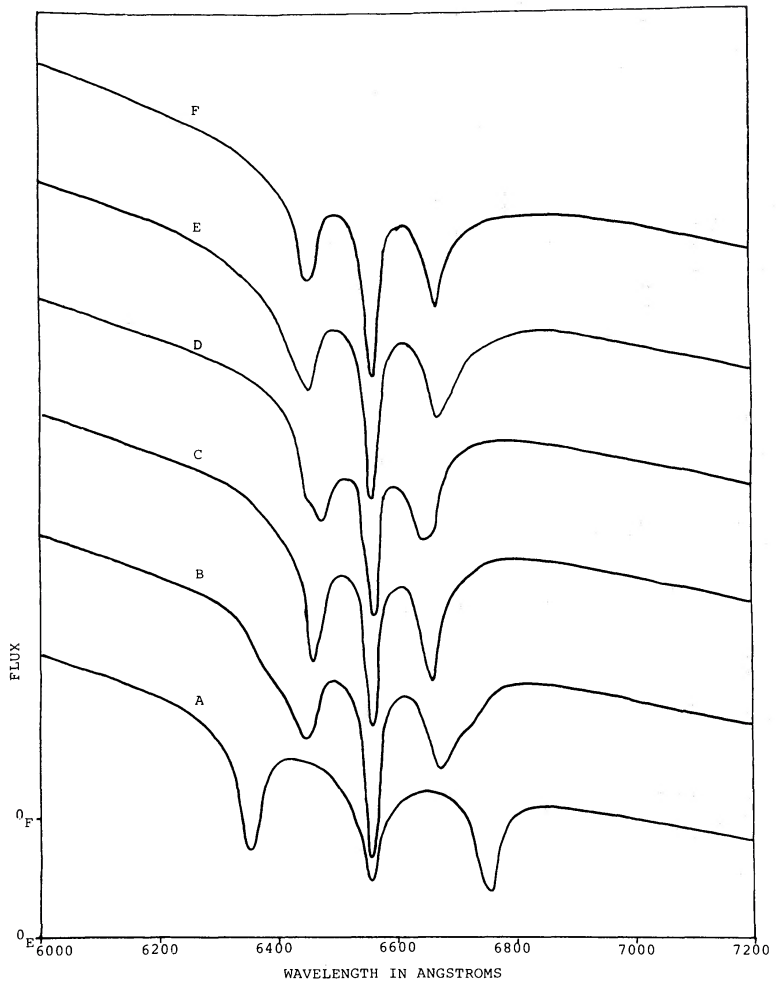

Figure 7. As Fig. 6, except that the star is viewed from the plane of the equator ($i = 90°$). Results for cases G and H are identical to those for E and F, respectively.

4 Results

To illustrate the effect of different field distributions on the spectra of magnetic white dwarfs, we present in Figs 6–10 the flux, linear polarization and circular polarization for the uniform field, centre dipole, quadrupole and octupole fields, and dipoles offset by plus or minus 0.1 and 0.2. Information about the line is contained in the figure captions. The calculations were carried out using the zero-field, high-gravity (log $g = 8.0$), $T_e = 20\,000$ K model atmosphere taken from Wickramasinghe (1972). The continuum is polarized following Lamb & Sutherland (1974), line shifts due to the magnetic field are taken from Kemic (1974b), and magneto-optical effects associated with the lines and with the continuum are incorporated (Martin & Wickramasinghe 1981, 1982). The integration through optical depths was carried out using the method of Martin & Wickramasinghe (1979b), and the results at different latitudes and longitudes were appropriately weighted and combined to give the net result.

As noted in Martin & Wickramasinghe (1982), when the large values of ρ_R and ρ_W associated with free–free transitions are introduced into the calculation, the results become much more sensitive to changes in parameters such as the opacities. In particular, the use of a finite set of latitudes – and hence also of magnetic field strengths – in integrating across the surface of the star can result in numerically induced bumps in the spectrum. One way of

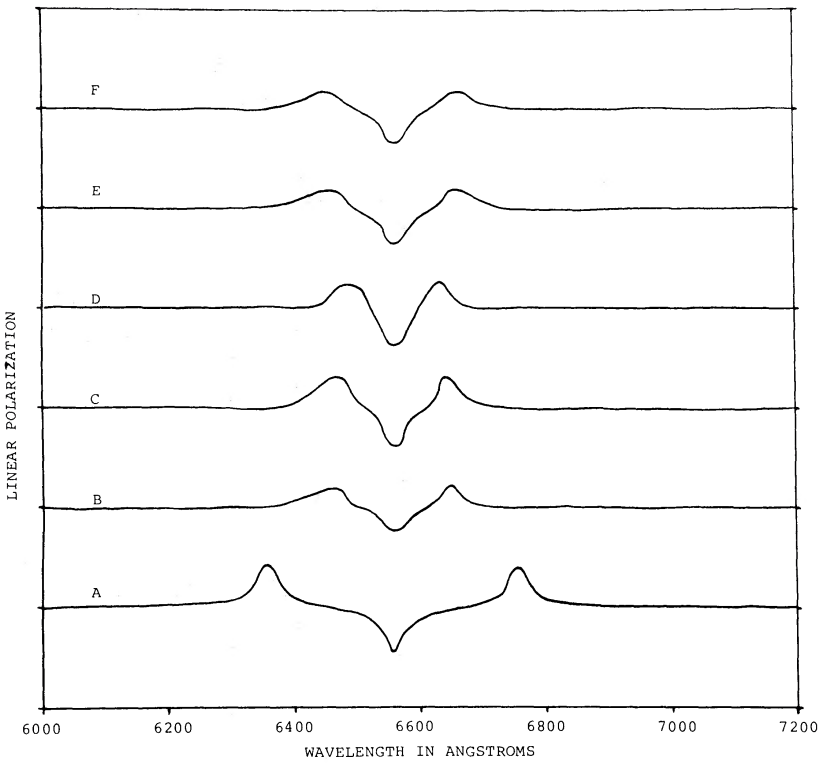

Figure 8. As Fig. 7, except that linear polarization is presented ($i = 90°$). Spacing between the curves represents a polarization of 10 per cent, except for the uniform field A in which this spacing represents 50 per cent. (Note that linear polarization for $i = 0°$ is identically zero, so no results are shown for this case.)

overcoming this problem is to increase the number of latitudes used in the numerical integration, but this increases computation time inordinately. For the calculations for this paper, the following approach was used. For each latitude ξ_i and optical depth, the variation in magnetic field strength associated with the latitude – namely, the variation in field strength from $\frac{1}{2}(\xi_{i-1} + \xi_i)$ to $\frac{1}{2}(\xi_i + \xi_{i+1})$ – was determined. Then the opacities and magneto-optical parameters associated with this range of field strengths were averaged, and these averages used in (1)–(7) to calculate the solution associated with the latitude ξ_i. This latitude averaging of opacities is in addition to an averaging of opacities associated with the set of wavelengths, spaced at 10 Å intervals, for which results are obtained.

Of course, this method is inaccurate to the extent that the solution to the radiative transfer equations for an average of opacities does not equal the average of the solutions for the range of opacities being averaged. The approximation is not too bad if the opacities averaged are not too different, and it does overcome much of the numerically induced bumpiness of the spectrum. The numerical integrations across the surface of the star were carried out using 24 latitudes from pole to pole (and somewhat more latitudes for offset dipoles with their greater range of magnetic field strengths), with up to 6 longitudes at each latitude. The opacity averaging method sometimes results in a slightly increased line depth. And because of its intrinsic limitations and other inaccuracies, polarization results should not be assumed to be accurate to better than 1 per cent. In particular, linear polarization is very sensitive to numerical approximations, and little reliance should be placed on small deviations in linear polarization results here.

The features in the lines in Figs 6 and 7 are in accordance with the rough analysis of field strengths given earlier, when account is taken of the viewing angle. In particular, in the

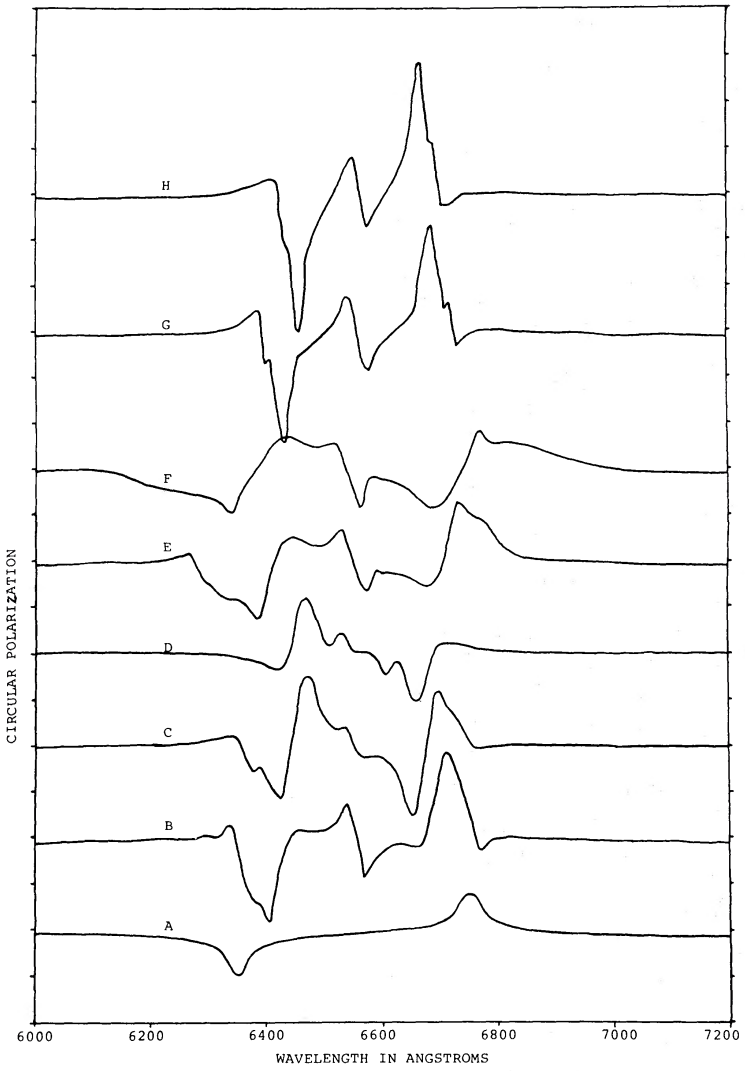

Figure 9. As Fig. 6, except that circular polarization is presented ($i = 0°$). The spacing between marks on the vertical axes represents a polarization of 5 per cent, except for the uniform field in which this spacing represents 25 per cent.

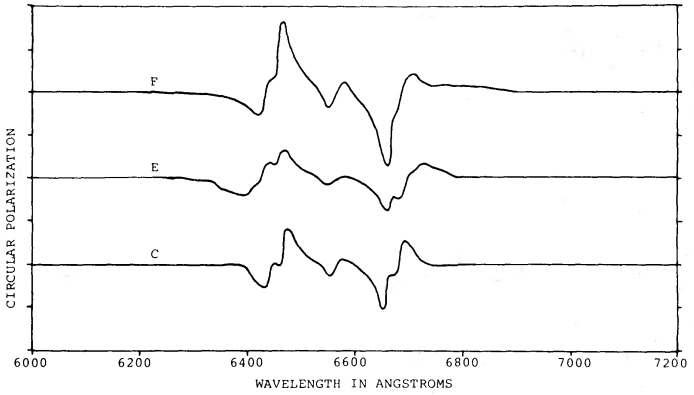

Figure 10. As Fig. 9, except that the star is viewed from the plane of the equator ($i = 90°$). Only results that are not identically zero are shown. Results for cases G and H are identical in magnitude but opposite in sign to those for E and F, respectively.

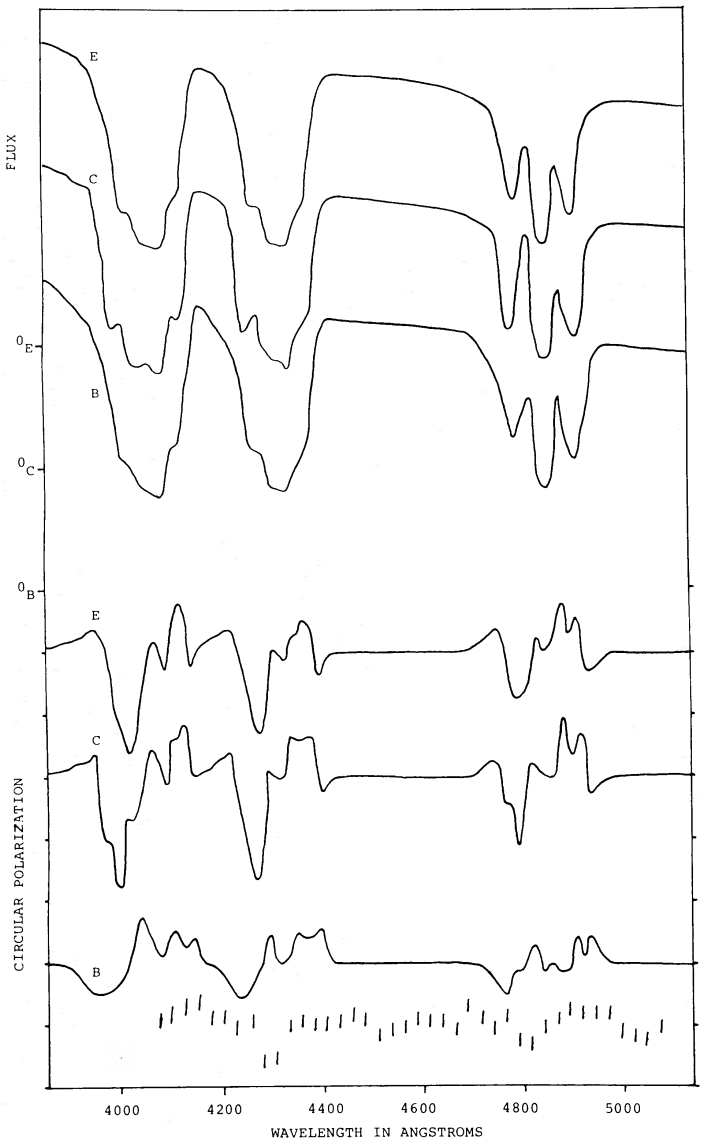

Figure 11. Flux (top) and circular polarization (bottom) for three models for magnetic white dwarf GD90. At the very bottom are the observations of the circular polarization for GD90 from Angel *et al.* (1974). The models are (B) centred dipole with dipole strength $B_d = 9 \times 10^6$ G and viewing angle $i = 75°$, (C) centred quadrupole with polar field strength $B_p = 1.2 \times 10^7$ G and $i = 90°$. and (E) dipole offset by 0.1 radius towards the north pole, with dipole field strength $B_d = 9 \times 10^6$ G and $i = 90°$. The polarity of the quadrupole has been reversed to show the similarity of circular polarization for models C and E. The $T_e = 12\,000$ K model atmosphere is taken from Wickramasinghe (1972). The distance between adjacent marks for circular polarization represents 10 per cent. The zeros for the flux curves are indicated.

pole-on case ($i = 0°$, Fig. 6), the features are narrower in the higher multipole fields and very much narrower in the dipoles offset away from the viewing angle, and are broader in the dipoles offset toward the viewing angle. For equator-on viewing ($i = 90°$, Fig. 7), the differences between the centred dipole, quadrupole and octupole are less marked since the high field polar regions make less contribution to the surface average (see Fig. 2) owing to projection effects.

The polarization curves (Figs 8–10) are more sensitive to field geometry since both the field direction and field strength are important. Again, the largest differences are seen in the pole-on ($i = 0°$) cases.

We note that the offset dipoles show a dipole type behaviour when viewed pole-on from the northern hemisphere, and a quadrupole type behaviour when viewed equator-on ($i = 90°$). This is a general property which we expect to be valid for small values of the offset parameter s.

To illustrate how these results might apply to particular stars, we consider the case of GD90. Previously (Wickramasinghe & Martin 1979) we found that an offset dipole gave a better fit than a centred dipole. In Fig. 11 we present three models for GD90: centred dipole, $B_p = 9 \times 10^6$ G, viewing angle $i = 75°$; dipole offset by $s = 0.1$, $B_d = 9 \times 10^6$ G, $i = 90°$; quadrupole, $B_p = 1.2 \times 10^7$ G, $i = 90°$. The polar field used for the quadrupole is higher than for the dipoles since the bulk of field strengths for the quadrupole are clustered at a lower fraction of the polar field strength (Fig. 3). To reproduce the observed magnitude of circular polarization, a viewing angle of 75° – slightly different from $i = 90°$ which gives zero circular polarization – is used for the centred dipole. The quadrupole and the offset dipole give non-non-zero circular polarization even at $i = 90°$ (Fig. 10).

Circular polarization data on GD90 is also reproduced in Fig. 11 (Angel *et al.* 1974). It is clear that the centred dipole cannot explain the data, and also that the quadrupole and offset dipole give very similar results. The data would have to be greatly refined, and also a large number of models with different parameters tested – and possibly a more detailed and comprehensive model developed – before there would be much chance of choosing between the quadrupole and offset dipole models. (For these reasons, Angel *et al.*'s flux data, which is even less useful than their circular polarization data for choosing between the models, is not presented in Fig. 11.)

Distinguishing between a combination of multipoles and an offset dipole would not be easy even with superb observational data, because of the great degree of flexibility the free parameters allowing in modelling. This is an important point, and hence we discuss briefly how agreement between theory and observation can be obtained.

To begin, the positions of the absorption components can usually be reproduced by appropriately choosing the strength of the magnetic field, as noted above. To distinguish between the dipole field and its alternatives, polarization data usually must be used. The magnitude of the dominant circular polarization features can be reproduced by choosing the appropriate viewing angle: nearer to zero for large magnitudes, closer to 90° for small polarization values. (For very small observed circular polarization values, theoretical models based on a quadrupole or on a dipole offset along its polar axis could be ruled out. But this would not rule out other non-dipole fields, such as an octupole or a dipole offset perpendicular to the polar axis.) The signs of all polarization features can be switched easily for all types of field distribution by flipping the direction of the source of the field.

The multipoles and the offset dipoles actually provide *too* much flexibility in modelling magnetic white dwarfs. For example, any linear combination of centred dipole and quadrupole might be considered, not to mention contributions from octupole and higher multipoles, and dipoles offset towards the pole by any fraction might be considered, not to mention offsetting perpendicular to the polar axis. By using this flexibility to the utmost, good fits between theory and observation probably can be obtained in many cases, but because of this flexibility this fit does not necessarily indicate the validity of the model parameters.

The above comments apply strictly to magnetic white dwarfs that are effectively non-rotating and are hence observed only at a fixed magnetic phase. Under certain circumstances it may be possible to study a slowly rotating magnetic white dwarf at different magnetic phases. Time resolved observations of such a system may provide sufficient additional constraints to enable a choice between multipole and offset dipole field geometries.

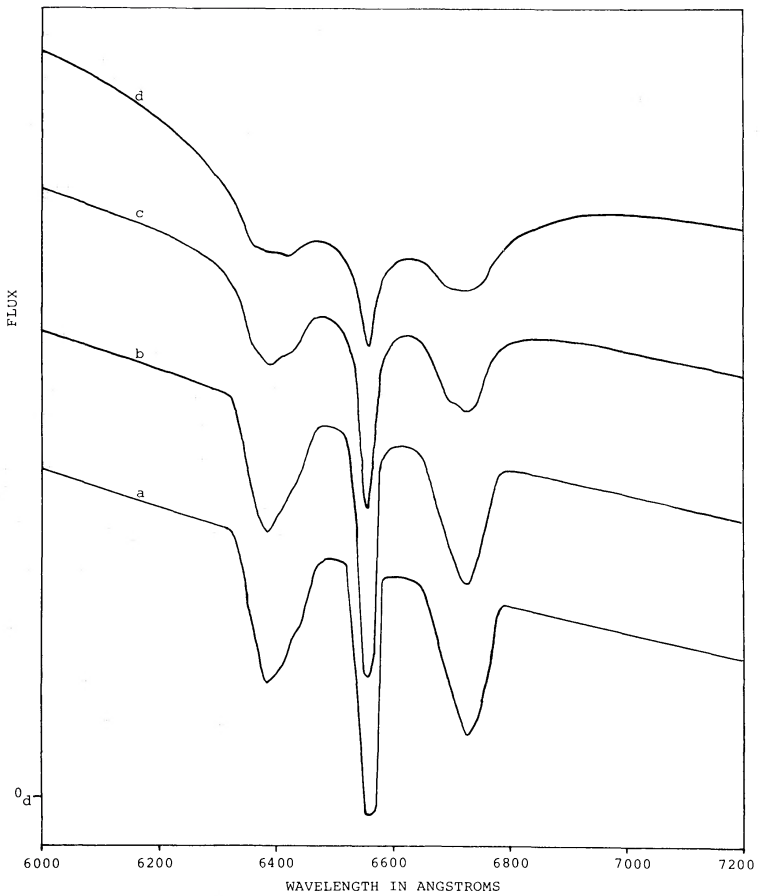

Figure 12. Flux values for the Zeeman triplet of Hα for four different values of pressure broadening. A centred dipole with $B_d = 10^7$G is assumed, with positions of the line components taken from Kemic (1974b). The $T_e = 20\,000$ K model atmosphere is taken from Wickramasinghe (1972). A Voigt line profile is assumed, with four values of the damping parameter a: (a) 0.001, (b) 0.01, (c) 0.1, (d) 1.0. The solution is calculated including magneto-optical effects.

5 Broadening

In general both pressure (usually Stark) and magnetic broadening must be included in models. Clearly when one type of broadening is much larger, the other may be neglected: for large magnetic fields and narrow lines pressure broadening may be neglected while for small magnetic fields, magnetic broadening may be neglected. Since the Stark widths of lines are strongly dependent on the atom and the transition involved, each case must be considered individually.

In our previous work which dealt mainly with hydrogen lines, Stark broadening was included assuming that the broadening was independent of the magnetic field. However, at sufficiently high magnetic fields, the l-degeneracy of the atomic hydrogen levels is removed by the quadratic Zeeman effect, and Stark broadening will be reduced. Unfortunately a determination has not been made of the Stark widths of the hydrogen components in the presence of a magnetic field. However, the effect of changing the Stark width on a Zeeman triplet can be seen from the results presented in Fig. 12. We note in particular the deepening of the lines as the Stark width is reduced until eventually magnetic broadening becomes the dominant broadening mechanism. Our failure in Wickramasinghe & Martin (1979) to match the depths of observed lines in GD90 and BPM 25114 is most probably due to an overesti-

mate of the Stark widths. This can be seen from the calculations in Fig. 11 in which the Stark width was reduced by a factor 100 relative to the zero field values. The triplet at Hβ is now clearly resolved as in the high resolution observations of Angel *et al.* (1974). It would appear that in the absence of independent information on the broadening, the Stark width is another free parameter whose variation can achieve better agreement between observation and model.

6 Conclusions

We have investigated the effects of magnetic field geometry on the spectroscopic and polarimetric properties of magnetic white dwarfs. With good quality spectropolarimetric observations it should in general be possible to recognize a white dwarf with a dominant centred dipole component even in the usual situation when data is available only at a single magnetic phase. However, when the observations indicate a departure from the centred dipole models, it will be difficult to distinguish between offset dipoles and combinations of multipoles except perhaps in rare situations when the white dwarf can be observed at different magnetic phases. For instance, in the case of GD90 we infer a non-centred dipole field distribution but on the basis of available data cannot distinguish between offset dipole and quadrupole fields.

We have also investigated the effect of line broadening on the spectra of magnetic white dwarfs. The observations of magnetic DA white dwarfs suggest that Stark broadening is much less than in the zero field case due to the removal of l-degeneracy.

References

Angel, J. R. P., 1978. *A. Rev. Astr. Astrophys.*, **16,** 487.

Angel, J. R. P., Carswell, R. F., Strittmatter, P. A., Beaver, E. A. & Harms, R., 1974. *Astrophys. J.*, **194,** L49.

Borra, E. F., 1976. *Astrophys. J.*, **209,** 858.

Cowan, E. W., 1968. *Basic Electromagnetism,* Academic Press, New York.

Hardorp, J., Shore, S. N. & Wittmann, A., 1976. *Physics of A_p Stars,* p. 419, eds Weiss, W. W., Jenkner, H. & Wood, H. J., Universitätssternwarte Wein, Vienna.

Kemic, S. B., 1974a. *Astrophys. J.*, **193,** 213.

Kemic, S. B., 1974b. Joint Institute Laboratory Astrophysics Report 113.

Lamb, F. K. & Sutherland, P. G., 1974. *Physics of Dense Matter,* p. 265, ed. Hansen, C. J., Reidel, Dordrecht, Holland.

Landstreet, J. D., 1979. *White Dwarfs and Variable Degenerate Stars,* p. 297, eds Van Horn, H. M. & Weidemann, V., University of Rochester Press, Rochester.

Landstreet, J. D., 1980. *Astr. J.*, **85,** 611.

Liebert, J., Angel, J. R. P., Stockman, H. S., Spinrad, & Beaver, E. A., 1977. *Astrophys. J.*, **214,** 457.

Martin, B. & Wickramasinghe, D. T., 1978. *Mon. Not. R. astr. Soc.*, **183,** 533.

Martin, B. & Wickramasinghe, D. T., 1979a. *Mon. Not. R. astr. Soc.*, **189,** 69.

Martin, B. & Wickramasinghe, D. T., 1979b. *Mon. Not. R. astr. Soc.*, **189,** 883.

Martin, B. & Wickramasinghe, D. T., 1981. *Mon. Not. R. astr. Soc.*, **196,** 23.

Martin, B. & Wickramasinghe, D. T., 1982. *Mon. Not. R. astr. Soc.*, **200,** 993.

O'Donoghue, D. E., 1980. *Astrophys. Space Sci.*, **68,** 273.

Ruderman, M. A. & Sutherland, P. G., 1973. *Nature,* **246,** 93.

Unno, W., 1956. *Publs astr. Soc. Japan,* **8,** 108.

Wegner, G., 1977. *Mon. Not. astr. Soc. Southern Africa,* **36,** 63.

Wickramasinghe, D. T., 1972. *Mem. R. astr. Soc.*, **76,** 129.

Wickramasinghe, D. T. & Martin, B., 1979. *Mon. Not. R. astr. Soc.*, **188,** 165.